Revision 2

The spin state of iron in Fe^{3+}-bearing Mg-perovskite and its crystal chemistry at high pressure

Izumi Mashino[1,*], Eiji Ohtani[1,2], Naohisa Hirao[3], Takaya Mitsui[4], Ryo Masuda[5], Makoto Seto[5], Takeshi Sakai[1,6], Suguru Takahashi[1], Satoshi Nakano[7]

[1]Department of Earth and Planetary Materials Science, Graduate School of Science, Tohoku University, Sendai 980-8578, Japan.

[2]V.S. Sobolev Institute of Geology and Mineralogy, Siberian Branch, Russian Academy of Sciences, Koptyuga Ave., 3, Novosibirsk, 630090, Russia

[3] Japan Synchrotron Radiation Institute, Sayo, Hyogo 679-5198, Japan.

[4]Japan Atomic Energy Agency, Sayo, Hyogo 679-5148, Japan.

[5] Research Reactor Institute, Kyoto University, Kumatori, Sennan-gun, Osaka 590-0494, Japan

[6]Geodynamics Research Center, Ehime University, Matsuyama 790-8577, Japan.

[7] National Institute for Materials Science, 1-1 Namiki, Tsukuba, Ibaraki 305-0044, Japan.

Abstract

Valence, spin states and crystallographic sites of Fe in (Mg,Fe)SiO_3 perovskite were investigated using energy-domain ^{57}Fe-synchrotron Mössbauer spectroscopy and powder X-ray diffraction up to 86 GPa. The volumes of Fe^{3+}-bearing perovskite in this study are slightly smaller than those of Mg-endmember perovskite. Our Mössbauer data suggest that Fe^{3+} prefers A sites coupled with Mg vacancies, which is consistent with previous data at ambient conditions. Fe^{3+} in the A site remains in a high spin state up to 86 GPa, and some fraction of the A site is occupied by Fe^{2+} at pressures above 30 GPa. Fe^{2+} in the A sites is also in a high spin state up to 86 GPa. The coupled substitution from Mg^{2+} to a high spin state of Fe^{3+} and Mg^{2+} vacancy would make the volume of perovskite smaller than that of Mg-endmember perovskite. If the lower mantle is saturated in silica, perovskite containing high spin Fe^{3+} in A site has a higher density. Such silica oversaturated regions could sink by the density difference.

Keywords: perovskite, ferric iron, spin state, Mössbauer spectroscopy, X-ray diffraction

Introduction

The Earth's lower mantle is composed mainly of iron-bearing magnesium silicate perovskite (Pv, $(Mg,Fe)SiO_3$) and ferropericlase (Fp, (Mg,Fe)O). The effects of iron in these mantle materials are fundamental to understanding the deep mantle (e.g., Stixrude *et al*., 1992). A spin transition in the lower mantle minerals can change several important physical properties of the deep lower mantle regions, such as the thermal conductivity and partitioning behavior between Mg and Fe (Badro *et al*., 2003; 2004). Previous studies (e.g., McCammon, 1997) revealed that a large amount of ferric iron Fe^{3+}, ca. ~50%, could exist in the lower mantle when aluminum is contained in Pv. Ferric iron in Pv influences the electrical conductivity and controls the thermal conductivity in the lower mantle (Xu *et al.*, 1998; Goncharov *et al.*, 2008; Keppler *et al.*, 2008).

By using nuclear forward scattering of synchrotron radiation, Catalli *et al.* (2010) reported that the population of the LS state of ferric iron Fe^{3+} in octahedral sites (hereafter B sites) of $(Mg, Fe^{3+})SiO_3$ gradually increases with pressure, and the spin transition becomes complete at 50–60 GPa. Grocholski *et al.* (2009) found that Fe^{2+} exists in two different environments, but both are likely HS along with Fe^{3+} in B sites

and possibly small amounts of LS Fe^{2+} and LS Fe^{3+} up to 65 GPa. In contrast, ferric iron Fe^{3+} in dodecahedral sites (hereafter A sites) remains in the HS state under conditions relevant to the lower mantle. Recently Lin *et al.* (2012) showed the HS to LS transition of Fe^{3+} in the B sites in the range of 13–24 GPa in Al-free (Mg, Fe)SiO_3-Pv. Additionally, some experimental studies have proposed that Fe^{3+} undergoes the HS to LS transition in Al-bearing Pv (Fujino *et al.*, 2012; Catalli *et al.*, 2011).

Computational studies have predicted that the LS state of Fe^{3+} in B sites of Pv is stable at lower mantle pressures and the HS-LS transition of Fe^{3+} in A sites occurs in the range from 60 to 150 GPa (Zhang and Oganov, 2006; Stackhouse *et al.*, 2007). According to recent calculations using density functional theory and the Hubbard parameter, Fe^{3+} in the B site of Pv undergoes a crossover from HS to LS state at 50–60 GPa, and Fe^{3+} in the A site remains in the HS state up to 150 GPa (Hsu *et al.*, 2012). In Pv structures, $A^{2+}B^{4+}O_3$, the incorporation of trivalent ions (M^{3+}) occurs by two mechanisms: $A^{2+} + B^{4+} = M^{3+} + M^{3+}$ and $B^{4+} = M^{3+} + 0.5V_O^{2+}$ (V_O^{2+}, oxygen vacancy) (Knight *et al.*, 1994; Navrotsky, 1999; Navrotsky *et al.*, 2003). Fe^{3+} should occupy both A and B sites in the Pv structure and these mechanisms must depend on other phases buffering Pv (McCammon, 1998; Catalli *et al*., 2010; Hsu *et al.*, 2011). McCammon (1998) suggested that the coupled substitution could occur: $2^BSi^4 + \leftrightarrow 2^BFe^{3+} + V_O^{2+}$ at

lower f_{O2} using a Re capsule whereas $^{A}Mg^{2+} + {}^{B}Si^{4+} \leftrightarrow {}^{A}Fe^{3+} + {}^{B}Fe^{3+}$ at higher f_{O2} using a Fe capsule. The charge-coupled substitution mechanism makes it hard to understand the behavior of Fe^{3+} in Pv. Based on NFS measurements in the time domain, Catalli *et al*. (2010) suggested that Fe^{3+} in Al-free Pv occupies both the A and B sites equally at high pressure and ambient temperature.

The behavior of Fe^{3+} in Pv is complex because it can occupy two nonequivalent sites in the crystal lattice. Thus, we conducted high-pressure energy-domain synchrotron ^{57}Fe-Mössbauer spectroscopy and *in situ* powder X-ray diffraction experiments (XRD) of Fe^{3+}-bearing Pv using a diamond anvil cell (DAC) to investigate the coordination sites that Fe^{3+} occupies in Al-free $(Mg,Fe)SiO_3$-Pv, and to clarify the spin state of iron and the effects of the HS-LS transition of iron on the pressure–volume (*P–V*) relationship.

Experimental Methods

^{57}Fe -enriched enstatite gel, as a starting material, was synthesized from tetraethyl orthosilicate $(C_2H_5O)_4Si$, magnesium nitrate $Mg(NO_3)_2{\cdot}6H_2O$, and powdered ^{57}Fe metal (96.63% enriched in ^{57}Fe) by a sol-gel method. The enstatite gel was heated in a gas furnace with CO_2 gas at 700 °C. The composition $(Mg_{0.91},Fe_{0.09})SiO_3$ was examined

using a scanning electron microscope with energy dispersive spectroscopy (Table 1). To prevent formation of other Fe-bearing phases, the amount of SiO_2 component exceeds that of the stoichiometry. The Fe^{3+} content ($Fe^{3+}/\Sigma Fe$) in the enstatite gel was measured by conventional ^{57}Fe-Mössbauer spectroscopy.

A symmetric-type DAC with a culet size of 130, 250, and 300 μm was used to generate high pressure. The enstatite gel with a thickness of 10 μm was coated on both sides with gold in ~300 nm thick. Gold serves as a pressure marker and a laser absorber in order to anneal the sample homogeneously and stably. The sample was loaded into a hole with 40–130 μm in diameter, drilled in a pre-indented Re gasket with 40 μm thickness. Neon was loaded into the DAC using a high-pressure gas-loading system (Takemura *et al*., 2001) and was used as a pressure medium and a pressure marker. The sample was placed on ruby chips, a few micrometers across, to avoid direct contact with the anvil culet. The deposited gold is also used to prevent ruby and the sample from reacting. The silicate Pv phase was synthesized from the enstatite gel at 30–40 GPa and 1800 K for 15 min through a double-sided laser heating technique using fiber lasers with a laser spot size of about 40 μm, and was confirmed by XRD.

The XRD experiments at high pressure were carried out using an angle-dispersive method at beamline BL10XU of SPring-8 (Ohishi *et al.*, 2008). A monochromatic X-ray

beam with wavelength of 0.4114 Å was focused down to 10 μm using the focusing optics of compound refractive lenses. XRD spectra were collected on an imaging plate with an exposure time of 3–5 min. Collected two-dimensional XRD patterns were analyzed using softwares, IPAnalyzer and PDIndexer (http://www2.kobe-u.ac.jp/~seto/) (Seto *et al.*, 2008).

Pressure was determined using the equation of state (EOS) of gold (Tsuchiya, 2003). Volumes of gold were calculated using the diffraction peaks of (111) and (002). In Run# Pv1006, however, the intensity of gold was not enough and the diffraction peaks could not be used for pressure determination. In this case, pressure was determined using the equation of state (EOS) of neon (Fei *et al.*, 2007) and normalized pressure to Au scale from Ne scale. Volumes of neon were calculated using the diffraction peaks of (111), (002), and (022). In the experimental run for Mössbauer measurements of "cold-compression Pv" which was not annealed after Pv synthesis, ruby was used as a pressure standard by measuring several points around the central area of the sample (Dewaele *et al*., 2004). Experimental details are summarized in Table 2.

Energy-domain SMS was carried out at BL11XU of SPring-8 (Mitsui *et al*., 2009). The focused X-rays from a broadband SR source are ultra-finely monochromated

to a bandwidth of neV order by a pure nuclear Bragg reflection (333) of a $^{57}FeBO_3$ single crystal. Mössbauer spectra were obtained using a NaI scintillation detector, and were typically collected for 6 h. Mössbauer spectra were fitted to the Lorentzian-squared line shape for synchrotron source (equal quadrupole component widths and areas) using the available fitting program *MossA* (Prescher *et al.*, 2012).

Result and Discussion

In situ powder x-ray diffraction

According to conventional ^{57}Fe-Mössbauer spectroscopy with a radioactive isotope source, iron in the enstatite gel was found to be present as follow (Table 3); two doublets with quadrupole splitting (QS) = 1.543(7) and isomer shift (IS) = 0.255(3), and QS = 0.877(5) and IS = 0.341(3) mm/s can be associated with Fe^{3+}, whereas one doublet with an extremely high QS = 2.524(9) and IS = 0.454(4) mm/s can be assigned to Fe^{2+} (e.g., Dyer, 1985; McCammon, 2004). The Fe^{3+} content ($Fe^{3+}/\Sigma Fe$) in the enstatite gel is around 90%.

We measured the volume of Fe^{3+}-bearing Pv synthesized from the gel starting material up to 86 GPa at ambient temperature using *in situ* powder XRD, except for Run# Pv1008. We also observed weak diffraction lines from stishovite (St) or

145 $CaCl_2$-type SiO_2. Synthesis of the Pv phase was confirmed after heating at 1800 K. We
146 confirmed the diffraction patterns from the orthorhombic Pv structure (space group:
147 *Pbnm*) with those of Au and Ne, as shown in Fig. 1. We again observed weak
148 diffraction lines from St and $CaCl_2$-type SiO_2 (Fig. 1). No diffraction lines from other
149 Fe-bearing minerals, including Fe_3O_4, Fe_2O_3, metallic Fe and Fp, were identified. The
150 bulk starting composition exceeds that of the enstatite stoichiometry; Si/(Mg+Fe) = 1.05
151 for atomic %.

152 The volumes and unit cell parameters of Fe^{3+}-bearing Pv and St or the $CaCl_2$-type
153 SiO_2 for each run are provided in Table 4. In total, 16 diffraction lines for Fe^{3+}-bearing
154 Pv and 5 diffraction lines for St or the $CaCl_2$-type SiO_2 were typically used to constrain
155 the volumes and unit cell parameters. We fit the measured *P–V* data to a second-order
156 Birch–Murnaghan (B–M) EOS (for a fixed pressure-derivative K'_0 of 4.0), based on the
157 Au scales by Tsuchiya (2003). Fitting all of the *P–V* data of St, we obtained a bulk
158 modulus of K_0 = 294(6) GPa with V_0 = 46.79(10) Å^3. The obtained K_0 and V_0 shows in
159 good agreement with previous studies (e.g., Nishihara *et al*., 2005; Wang *et al.,* 2012).
160 The obtained parameters of Fe^{3+}-bearing Pv can be reliably extracted from the data of
161 St.

162 From the *P–V* relationships of Fe^{3+}-bearing Pv, there is no discontinuous change in

the trend of volumes and unit cell parameters with pressure by annealing at 1800 K (Fig. 2). We also fit the measured *P–V* data of Fe^{3+}-bearing Pv to a second-order B–M EOS, based on the Au scales by Tsuchiya (2003). To compare the volumes of all data, pressures of Run# Pv1006 were normalized to the Au scale from the Ne scale (Fig. 2). Fitting all of the *P–V* data conducted after annealing between 31 and 86 GPa to the B–M EOS, we obtained a bulk modulus of K_0 = 265±6 GPa with V_0 = 161.43±0.44 $Å^3$. Compared with the volumes of Mg-endmember and Fe^{2+}-bearing Pv, $(Mg_{0.91}Fe^{2+}_{0.09})SiO_3$ measured by Lundin *et al*. (2008), those of Fe^{3+}-bearing Pv in this study are slightly smaller than both Mg-endmember Pv and Fe^{2+}-bearing Pv (Table 5). The K_0 of Fe^{3+}-bearing Pv matches well, within the uncertainty, with Mg-endmember Pv using the same Au scale. The volumes of Fe^{3+}-bearing Pv measured by Catalli *et al*. (2010) are higher than those of Fe^{3+}-bearing Pv in this study. This volume decrease could be caused by the presence of Mg^{2+} vacancies in the synthesized Fe^{3+}-bearing Pv. When Fe^{3+} in the A site is accommodated by Mg^{2+} vacancies, the unit cell volumes of Fe^{3+}-bearing Pv could become smaller than Mg-endmember Pv. Detailed discussions on the substitution mechanism in Pv are below.

Energy-domain synchrotron Mössbauer spectroscopy

The unit cell volumes of Fe^{3+}-bearing Pv are slightly smaller than those of Mg-endmember Pv. Our Mössbauer data suggest that Fe^{3+} prefers A sites coupled with Mg vacancies, which is consistent with previous data at ambient conditions (Hummer and Fei, 2012). The coupled substitution could make the volume of Pv smaller than that of Mg-endmember Pv.

Energy-domain SMS was performed on all runs. Mössbauer spectra of Fe^{3+}-bearing Pv could be fitted to three doublets, all with positive IS relative to a α-^{57}Fe metal and QS. Three-doublet model was proposed in order to explain distortion of the dodecahedra (Fei *et al.*, 1994; Hummer and Fei, 2012). We suggest that a similar phenomenon occurs for Fe^{3+} in this study and also adopt the model. The experimental spectra and three component fits are shown in Fig. 3. The hyperfine parameters from fitting of data are also shown in Fig. 4 (Table 6).

The IS depends on the band distance, so a low IS value implies a short band distance. The IS values of Site 2 and Site 3 indicate to the HS state of Fe^{3+}, based on those of rock-forming minerals (e.g., McCammon *et al*., 2004).

Among the three doublets, the hyperfine parameters for Site 1 are larger than those of the other sites. Catalli *et al*. (2010) measured the time-domain SMS, XES, and XRD of $(Mg,Fe^{3+})(Fe^{3+},Si)O_3$Pv, and suggested that Fe^{3+} occupies the A and B sites equally.

199 They also indicated that Fe^{3+} at B site undergoes a HS to LS transition at 50–60 GPa,
200 while Fe^{3+} at A site remains in HS up to at least 135 GPa. In this study, however, Site 1
201 has QS values from 2.79 to 4.13 mm/s and IS values from 0.93 to 1.10 mm/s. The IS of
202 Site 1 is typically 1.0 mm/s. The IS value of Site 1 has characteristics of Fe^{2+}, and the
203 high QS value (>3.5 mm/s) also refers to HS of Fe^{2+} in the A site based on Grocholski
204 *et al*. (2009) and Lin *et al*. (2012). Therefore, Site 1 is identified as HS of Fe^{2+} in the A
205 site of Pv. Site 3 has hyperfine parameters characteristic of HS of Fe^{3+} in the distorted
206 dodecahedral site (A site) and Site 2 also has hyperfine parameters characteristic of HS
207 of Fe^{3+} in the A site. This is in good agreement with the experimental study of Hummer
208 and Fei (2012). They suggested that Fe^{3+} substitution causes a population of distorted
209 dodecahedral sites based on the behavior of Fe^{2+} in the A sites of Pv observed by Fei *et*
210 *al.* (1994) and McCammon *et al.* (2004). They also proposed that when the Fe^{3+}
211 concentration becomes higher (e.g., 7.4 mol %), Fe^{3+} in the A sites is accommodated by
212 Mg^{2+} vacancies ($3^{A}Mg^{2+} \rightarrow 2^{A}Fe^{3+} + V_{cation}$). These mechanisms could have occurred in
213 this study. Our data suggest that Fe^{3+} prefers A sites coupled with Mg vacancies
214 because of high Fe^{3+} concentrations and Fe^{3+} in A sites remains in the HS state up to 86
215 GPa. We also observed some Fe^{2+} atoms are accommodated in A sites and remain in the
216 HS state above 30 GPa, perhaps some reducing reactions in the sample might have

217 occurred in DAC by annealing. On the other hand, there is no change in either spin state
218 or oxidation state of cold-compression Pv. By annealing, the amount of Fe^{3+} in the
219 distorted A sites seems to increase with pressure above 40 GPa. In contrast, that of Fe^{3+}
220 in A sites decreases above 40 GPa (Fig. 4(c)). These parameters are different between
221 the sample with annealing and the cold-compression sample. This means that it is
222 important to realize the effect of temperature for the discussion of the spin state of iron
223 in the mantle, which is also indicated by previous studies (Grocholski *et al*., 2009;
224 Fujino *et al.,* 2012). We observed no evidence for the existence of Fe^{3+} in the B sites of
225 Pv, which had been indicated by Catalli *et al.* (2011). There is no change in the spin
226 state of cold-compression Pv in the pressure range studied in this work. These results
227 indicate that the spin state of iron in A sites of Pv does not change and remains as a HS
228 state below 85 GPa in the sample with annealing and cold-compression.

229 The crystal ionic radii of Mg, Si, Fe^{2+}, and Fe^{3+} are 1.03 Å (Mg^{2+} in A site), 0.54 Å
230 (Si^{4+} in B site), 1.06 Å (HS/Fe^{2+} in A site), 0.92 Å (HS/Fe^{3+} in A site), 0.79 Å (HS/Fe^{3+}
231 in B site), and 0.69 Å (LS/Fe^{3+} in B site), respectively (Shannon, 1976; Kudoh *et al.*,
232 1990). Hummer and Fei (2012) suggested that the relative doublet abundances of Fe^{3+} in
233 B sites is 50% and the substitution of Fe^{3+} in B site (0.79 Å) for Si^{4+} in B site (0.54 Å) is
234 a much larger increase in site radius than that of Fe^{2+} in A site (1.06 Å) for Mg^{2+} in A

site (1.03 Å). Thus, the presence of Fe^{3+} in a B site increases the unit cell volume substantially compared to that of the pure structure. In this study, the relative doublet abundances of Site 2 + Site 3, the HS of Fe^{3+} in A site, is over 66%. The HS crystal ionic radius of Fe^{3+} in A sites (0.92 Å) is smaller than Mg^{2+} in A sites (1.03 Å), while the HS crystal ionic radius of Fe^{2+} in A sites (1.06 Å) is larger than Mg^{2+} in A sites. When Fe^{3+} in the A sites is accommodated by Mg^{2+} vacancies, the unit cell volumes of Fe^{3+}-bearing Pv could become slightly smaller than Mg-endmember Pv. The content of Fe in A site has a linear relation with the volumes of Fe^{3+}-bearing Pv (Hemley and Cohen, 1992; Hummer and Fei, 2012). When the composition is $(Mg_{0.9},Fe_{0.1})SiO_3$ in Kudoh *et al.* (1990), the influence of Fe^{2+} and Fe^{3+} to the volume of Pv are +0.62 $Å^3$ and -2.27 $Å^3$, respectively. In the case of Run# Pv1006 at 41.4 GPa, the relative doublet abundances of Fe^{2+}:Fe^{3+} is 34:66. Taking into account of the composition of $(Mg_{0.91},Fe_{0.09})SiO_3$ in this study, the volume changes by Fe^{2+} and Fe^{3+} are +0.62 $Å^3$*(0.09/0.1)*34 % ≈ +0.19 $Å^3$, -2.27 A^3*(0.09/0.1)*66 % ≈ -1.35 $Å^3$, respectively. Therefore, Fe^{2+} and Fe^{3+} in A sites induce a unit cell volume reduction of roughly –1.16 $Å^3$. This reduction is in good agreement with the decreased volumes of Fe^{3+}-bearing Pv by XRD.

Implications

The Earth's mantle contains both ferric and ferrous iron. In the bulk mantle, Fe_2O_3 concentrations are estimated to be low in the upper mantle and transition zone, but high in the lower mantle (McCammon, 1997; 2005). Frost *et al*. (2004) showed that Fe^{3+} must form in the lower mantle by the disproportionation of Fe^{2+} to Fe^{3+} and metallic Fe. For Al-free $Mg_{0.94}Fe_{0.06}SiO_3Pv$, the amount of Fe^{3+} is found to be 16 ± 3 % (McCammmon, 1998). Hummer and Fei (2012) proposed that when Si > Mg, excess Fe^{3+} in A site is accommodated by Mg^{2+} vacancies ($3^AMg^{2+} \rightarrow 2^AFe^{3+} + V_{cation}$) at ambient condition. Our data also suggest that Fe^{3+} prefers A sites coupled with Mg vacancies in excess of Si.

We suggest that Fe^{3+} in perovskite prefers A sites coupled with Mg vacancies because of high Fe^{3+} concentrations if the lower mantle is saturated in silica. Fe^{3+} in A sites remains in the HS state up to 86 GPa. Fe^{2+} can also be accommodated in A sites and the Fe^{2+} ions in A sites are in the HS state to the same pressure. We compared the bulk moduli of perovskites with different compositions using the EOS fitting results (Table 5). The zero pressure volume and bulk modulus of Fe^{3+}-Pv are very close to those of Mg-Pv (Lundin *et al.*, 2008) and the spin transition of iron does not occur in our composition. Thus, the small volume and high spin state of iron in perovskite

observed in this work provides important implications for the physical properties in the lower mantle, i.e., if the lower mantle is saturated in silica, Pv containing Fe^{3+} in A site has a higher density and could contribute to the seismic velocity. Such silica oversaturated regions could sink in the lower mantle by the density difference.

Acknowledgements

We thank Prof. M. Akasaka at Shimane University for Mössbauer spectroscopy measurement of starting materials and Prof. K. Fujino at Ehime University for useful discussions. We also thank Drs. S.Kamada, T.Sakamaki, M.Hamada, I.Ohira, N.Nishitani, T.Sakairi, and M.Murakami of Tohoku University for their technical assistance and useful discussions. We also thank Dr. B. Mysen of Carnegie Institution of Washington for useful discussion for improving this manuscript. The synchrotron radiation Mössbauer spectroscopy measurements were performed at BL11XU in SPring-8 and the compression experiments were performed at BL10XU in SPring-8. This work was supported by JSPS KAKENHI Grant Numbers 18104009 and 22000002 awarded to E.O. This work was also partly supported by the Ministry of education and science of Russian Federation, project No 14.B25.31.0032 awarded to E.O. This work was conducted as part of the Global Center of Excellence program of Tohoku University

289 “Global Education and Research Center for Earth and Planetary Dynamics”.

290

291 **References**

292 Badro, J., Fiquet, G., Guyot, F., Rueff, J.-P., Struzhkin, V.V., Vankó, G., and Monaco,
293 G. (2003) Iron partitioning in Earth's mantle: toward a deep lower mantle
294 discontinuity. *Science*, 300, 789–791.

295

296 Badro, J., Rueff, J.-P., Vankó, G., Monaco, G., Fiquet, G., and Guyot, F. (2004)
297 Electronic transitions in perovskite: possible nonconvecting layers in the lower
298 mantle. *Science*, 305, 383–386.

299

300 Catalli, K., Shim, S.-H., Prakapenka, V.B., Zhao, J., Sturhahn, W., Chow, P., Xiao, Y.,
301 Liu, H., Cynn, H., and Evans, W.J. (2010) Spin state of ferric iron in $MgSiO_3$
302 perovskite and its effect on elastic properties. *Earth and Planetary Science Letters*,
303 289, 68–75.

304

305 Catalli, K., Shim, S.-H, Dera , P., Prakapenka, V.B., Zhao, J., Sturhahn, W., Chow, P.,
306 Xiao, Y., Cynn, H., and Evans, W.J. (2011) Effects of the Fe^{3+} spin transition on
307 the properties of aluminous perovskite—New insights for lower-mantle seismic

heterogeneities. *Earth and Planetary Science Letters*, 310, 293–302.

Dewaele, A., Loubeyre, P., and Mezouar, M. (2004) Equations of state of six metals above 94 GPa. *Physical Review B*, 70, 094112.

Dyar, M.D. (1985) A review of Mössbauer data on inorganic glasses: the effects of composition on iron valency and coordination. *American mineralogist*, 70, 304–316.

Fei, Y., Virgo, D., Mysen, B.O., Wang, Y., and Mao, H.K. (1994) Temperature-dependent electron delocalization in $(Mg,Fe)SiO_3$ perovskite. *American Mineralogist*, 79, 826–837.

Fei, Y., Ricolleau, A., Frank, M., Mibe, K., Shen, G., and Prakapenka, V. (2007) Toward an internally consistent pressure scale. *Proceedings of the National Academy of Sciences of the United States of America*, 104, 9182–39186.

Fujino, K., Nishio-Hamane, D., Seto, Y., Sata, N., Nagai, T., Shinmei, T., Irifune, T.,

Ishii, H., Hiraoka, N., Cai, Y., and Tsue, K.-D.(2012) Spin transition of ferric iron in Al-bearing Mg perovskite up to 200 GPa and its implication for the lower mantle. *Earth and Planetary Science Letters*, 317-318, 407–412.

Goncharov, A.F., Haugen, B.D., Struzhkin, V.V., Beck, P., and Jacobsen, S.D. (2008) Radiative conductivity in the Earth's lower mantle. *Nature*, 456, 231–234.

Grocholski, B., S. H. Shim, W. Sturhahn, J. Zhao, Y. Xiao, and P. C. Chow (2009) Spin and valence states of iron in $(Mg_{0.8}Fe_{0.2})SiO_3$ perovskite. *Geophysical Research Letters*, 36, L24303.

Hemley, R.J. and Cohen, R.E. (1992) Silicate Perovskite. *Annual Review of Earth and Planetary Sciences,* 20, 553–600.

Hsu, H., Blaha, P., Cococcioni, M., and Wentzcovitch, R.M. (2011) Spin-State Crossover and Hyperfine Interactions of Ferric Iron in $MgSiO_3$ Perovskite. *Physical Review Letters*, 106, 118501.

Hsu, H., Yu, Y. G., and Wentzcovitch, R.M. (2012) Spin crossover of iron in aluminous $MgSiO_3$ perovskite and post-perovskite. *Earth and Planetary Science Letters*, 359–360, 34–39.

Hummer, D.R. and Fei, Y. (2012) Synthesis and crystal chemistry of Fe^{3+}-bearing $(Mg,Fe^{3+})(Si,Fe^{3+})O_3$perovskite. *American Mineralogist*, 97, 1915–1921.

Keppler, H., Dubrovinsky, L.S., Narygina, O., and Kantor, I. (2008) Optical absorption and radiative conductivity of silicate perovskite to 125gigapascals. *Science*, 322, 1529–1532.

Knight, K.S. and Bonanos, N.J. (1994) Space Group and Lattice Constants for Barium Cerate and Minor Corrections to the Crystal Structures of $BaCe_{0.9}Y_{0.1}O_{2.95}$ and $BaCe_{0.9}Gd_{0.1}O_{2.95}$. *Journal of Materials Chemistry*, 4, 899–90.

Kudoh, Y., Prewitt, C.T., Finger, L.W., Darovskikh, A., and Ito, E. (1990) Effect of iron on the crystal structure of $(Mg,Fe)SiO_3$ perovskite. *Geophysical Research Letters*, 17, 1481–1484.

Lin, J.-F., Alp, E.E., Mao, Z., Inoue, T., McCammon, C., Xiao, Y., and Chow, J. (2012) Electronic spin states of ferric and ferrous iron in the lower-mantle silicate perovskite. *American Mineralogist*, 97, 592–597.

Lundin, S., Catalli, K., Santillán, J., Shima, S.-H., Prakapenkab, V.B., Kunzc, M., and Meng, Y. (2008) Effect of Fe on the equation of state of mantle silicate perovskite over 1 Mbar. *Physics of the Earth and Planetary Interiors*, 168, 97–102.

McCammon, C. (1997) Perovskite as a possible sink for ferric iron in the lower mantle. *Nature*, 387, 694–696.

McCammon, C. (1998) The crystal chemistry of ferric iron in $Fe_{0.05}Mg_{0.95}SiO_3$ perovskite as determined by Mössbauer spectroscopy in the temperature range 80–293 K. *Physics and Chemistry of Minerals*, 25, 292–300.

McCammon, C. (2004) Mössbauer spectroscopy: applications. *In Spectroscopic Methods in Mineralogy (A. Beran & E. Libowitzky, eds.) EMU Notes in*

Mineralogy, 6, 369–398.

McCammon, C. (2005) The paradox of mantle redox. *Science*, 308, 807–808.

Mitsui, T., Hirao, N., Ohishi, Y., Masuda, R., Nakamura, Y., Enoki, H., Sakaki, K., and Seto, M. (2009) Development of an energy–domain ^{57}Fe–Mössbauer spectrometer using synchrotron radiation and its application to ultrahigh–pressure studies with a diamond anvil cell. *Journal of Synchrotron Radiation*, 16, 723–729.

Navrotsky, A. (1999) A lesson from ceramics. *Science*, 284, 1788–1789.

Navrotsky, A., Schoenitz, M., Kojitani, H., Xu, H.W., Zhang, J.Z., Weidner, D.J., and Jeanloz, R. (2003) Aluminum in magnesium silicate perovskite: formation, structure, and energetics of magnesium-rich defect solid solutions. *Journal of Geophysical Research*, 108(B7), 2330.

Nishihara, Y., Nakayama, K., Takahashi, E., Iguchi, T., and Funakoshi, K. (2005) *P-V-T* equation of state of stishovite to the mantle transition zone conditions.

Physics and Chemistry of Minerals, 31, 660–670.

Ohishi, Y., Hirao, N., Sata, N., Hirose, K., and Takata, M. (2008) Highly intense monochromatic X–ray diffraction facility for high–pressure research at SPring–8. *High Pressure Research*, 28, 163–173.

Prescher, C., McCammon, C., and Dubrovinsky, L. (2012) *MossA*: a program for analyzing energy-domain Mössbauer spectra from conventional and synchrotron sources. *Journal of Applied Crystallography*, 45, 329-331.

Seto, Y., Hamane, D., Nagai, T. and Fujino, K. (2008) Fate of carbonates within oceanic plates subducted to the lower mantle, and a possible mechanism of diamond formation. *Physics and Chemistry of Minerals,* 35, 223.

Shannon, R.D. (1976) Revised effective ionic radii and systematic studies of inter atomic distances in halides and chalcogenides. *ActaCrystallographica Section A: Foundations of Crystallography*, 32, 751–767.

Stackhouse, S., Brodolt, J. P., and Price, G. D. (2007) Electronic spin transitions in iron-bearing $MgSiO_3$ perovskite. *Earth and Planetary Science Letters,* 253, 282–290.

Stixrude, L., Hemley, R. J., Fei, Y., and Mao, H.K.(1992) Thermoelasticity of Silicate Perovskite and Magnesiowüstite and Stratification of the Earth's Mantle. *Science*, 257, 1099–1101.

Takemura, K., Sahu, P.C., Yoshiyasu, K., and Yasuo, T. (2001) Versatile gas-loading system for diamond-anvil cells. *Review of Scientific Instruments*, 72, 3873–3876.

Tsuchiya, T. (2003) First-principles prediction of the P-V-T equation of state of gold and the 660-km discontinuity in Earth's mantle. *Journal of Geophysical Research*, 108 (B7), 2462.

Wang, F., Tange, Y., Irifune, T., and Funakoshi, K. (2012) *P-V-T* equation of state of stishovite up to mid-lower. *Journal of Geophysical Research*, 117(B0), 6209.

Xu, Y., McCammon, C., and Poe, B.T. (1998) The effect of alumina on the electrical

conductivity of silicate perovskite. *Science*, 282, 922–924.

Zhang, F. and Oganov, A.R. (2006) Valence state and spin transitions of iron in Earth's mantle silicates. *Earth and Planetary Science Letters*, 249, 436–443.

439

440 **Figure caption**

441

442 **Figure 1:** XRD pattern of Fe^{3+}–bearing Pv synthesized from gel starting material at 33
443 GPa and 1800 K (Run# Pv1006). This powder pattern is typical of all samples. Intensity
444 was normalized by that of Pv(112).

445 **Figure 2:** (a) Measured volume of Fe^{3+}–bearing Pv in this study (black circles;
446 Run#Pv1006, open circles; Run# Pv0606) and compression curves of Mg–end member
447 Pv, Fe^{2+}–bearing Pv, and Fe^{3+}–bearing Pv. The solid line is the fit to the second order
448 B–M EOS for Fe^{3+}–bearing Pv in this study. The dotted line is the EOS of Mg–end
449 member Pv and the dashed line is the EOS of Fe^{2+}–bearing Pv (Lundin *et al*., 2008). (b)
450 Unit cell parameters of Fe^{3+}–bearing Pv in this study (black circles; a axis of
451 Run#Pv1006, open circles; a-axis of Run#Pv0606, black triangles; b-axis of
452 Run#Pv1006, open triangles; b-axis of Run#Pv0606, black squares; c-axis of
453 Run#Pv1006, open squares; c-axis of Run#Pv0606). Pressure was determined using the
454 Au pressure scale by Tsuchiya (2003).

455 **Figure 3:** The synchrotron Mössbauer spectra of Fe^{3+}–bearing Pv at high pressures; (a)
456 with annealing; Run#Pv1006 (85 GPa) and (b) cold-compression; Run#Pv1008 (33
457 GPa). The spectrum was fitted with a three–doublet model, two assigned to Fe^{3+} in the

458 A site and one to Fe^{2+} in the A site.

459 **Figure 4:** Mössbauer parameters of Fe^{3+} in Fe^{3+}–bearing Pv. Black triangles; Site 1,

460 blue squares Site 2, red circles; Site3. Site 1 can be assigned to Fe^{2+} in A site of

461 perovskite, Site 2 to Fe^{3+} in A site, and Site 3 to Fe^{3+} in distorted A site in perovskite. (a)

462 isomer shifts, (b) quadrupole splitting, (c) percent weightings, (d) FWHM of Site 1, Site

463 2, and Site 3 for Run# Pv1006 with annealing. Pressure was determined using the EOS

464 of Au (Tsuchiya, 2003).

465

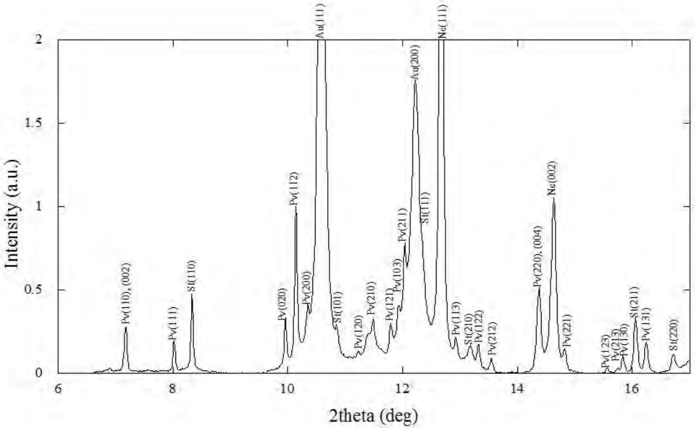
Intensity (a.u.)
2theta (deg)
0
0.5
1
1.5
2
6
8
10
12
14
16
Pv(110), (002)
Pv(111)
St(110)
Pv(020)
Pv(112)
Pv(200)
Au(111)
St(101)
Pv(120)
Pv(210)
Pv(121)
Pv(103)
Pv(211)
Au(200)
St(111)
Ne(111)
Pv(113)
St(210)
Pv(122)
Pv(212)
Pv(220), (004)
Ne(002)
Pv(221)
Pv(123)
Pv(213)
Pv(130)
St(211)
Pv(131)
St(220)

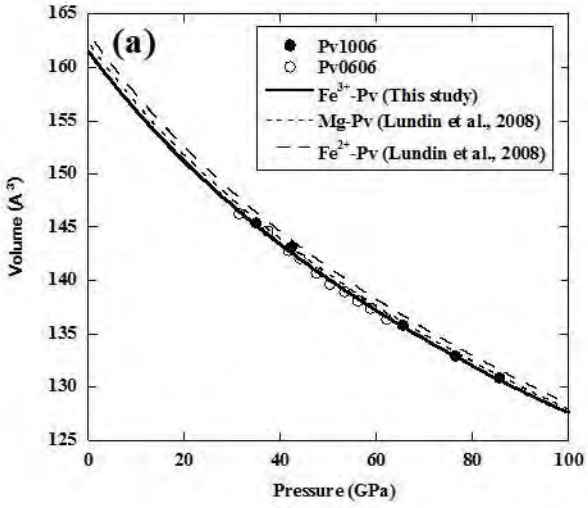
(a)
Pv1006
Pv0606
Fe3+-Pv (This study)
Mg-Pv (Lundin et al., 2008)
Fe2+-Pv (Lundin et al., 2008)
Volume (A3)
Pressure (GPa)
165
160
155
150
145
140
135
130
125
0
20
40
60
80
100

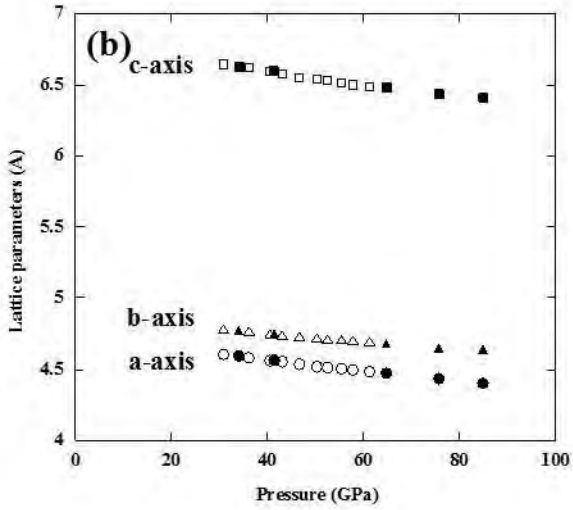
(b)
c-axis
b-axis
a-axis
Lattice parameters (A)
Pressure (GPa)
7
6.5
6
5.5
5
4.5
4
0
20
40
60
80
100

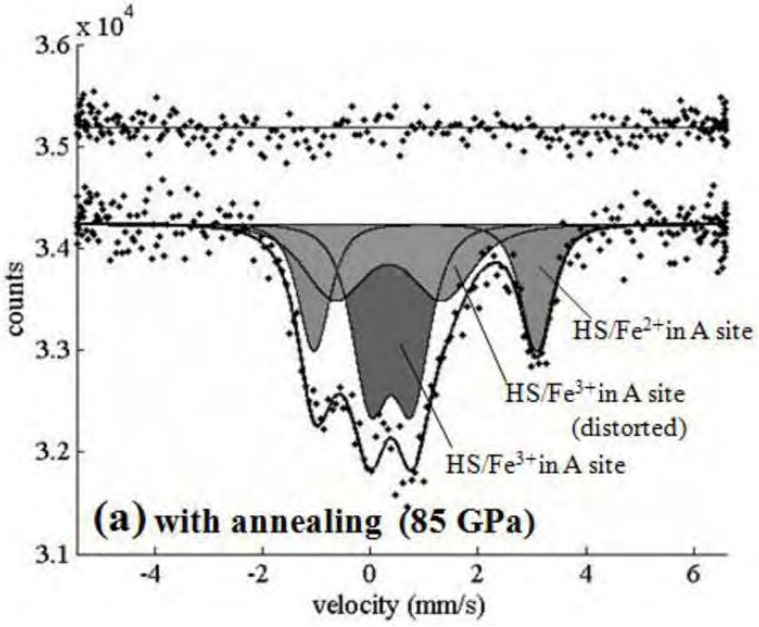
x 10^4
3.6
3.5
3.4
3.3
3.2
3.1
counts
-4
-2
0
2
4
6
velocity (mm/s)
HS/Fe2+in A site
HS/Fe3+in A site
(distorted)
HS/Fe3+in A site
(a) with annealing (85 GPa)

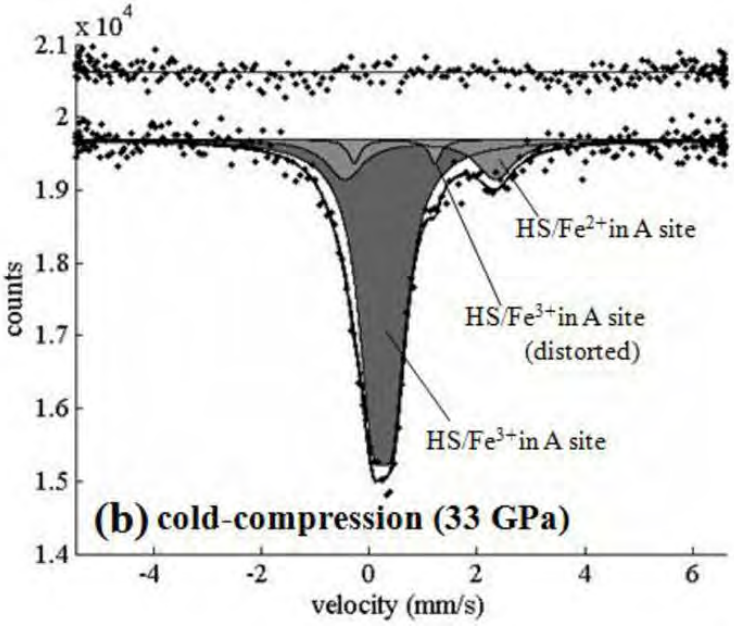
x 10^4
2.1
2
1.9
1.8
1.7
1.6
1.5
1.4
counts
-4
-2
0
2
4
6
velocity (mm/s)
HS/Fe2+in A site
HS/Fe3+in A site
(distorted)
HS/Fe3+in A site
(b) cold-compression (33 GPa)

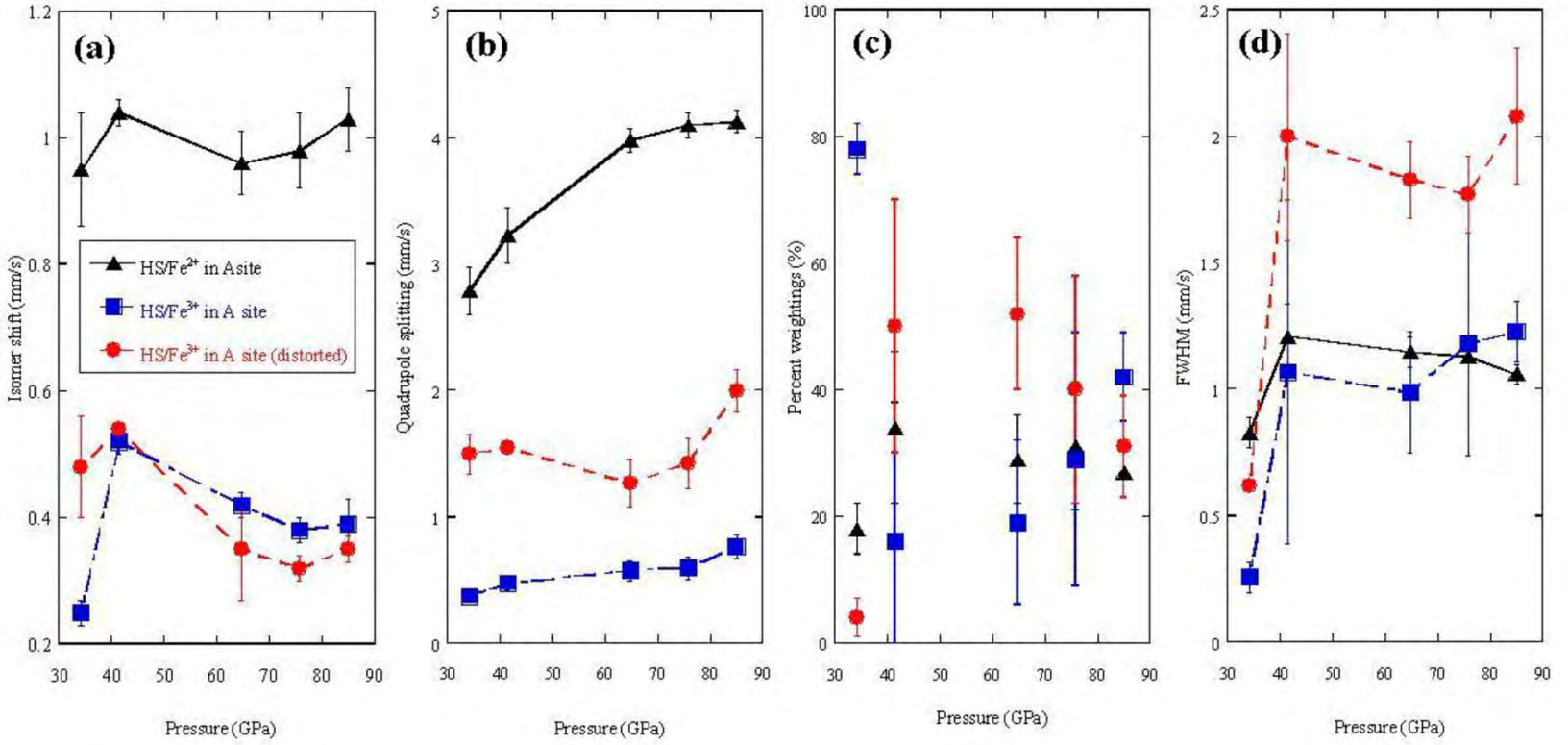
(a)
(b)
(c)
(d)
Isomer shift (mm/s)
Quadrupole splitting (mm/s)
Percent weightings (%)
FWHM (mm/s)
Pressure (GPa)
HS/Fe2+ in A site
HS/Fe3+ in A site
HS/Fe3+ in A site (distorted)

Table 1 Microprobe composition of ^{57}Fe-enriched enstatite gel

Elements	Weight %	Atomic %
SiO_2	59.3(4)	51.2(4)
MgO	34.5(3)	44.5(4)
Fe_2O_3	6.1(1)	4.4(1)
Al_2O_3	-	-
total	100	100

Table 2 The experimental details.

RUN#	Pressure scale	annealing	experiments
Pv1006	Ne(Fei2007)	with annealing	XRD & SMS
Pv0606	Au(Tsuchiya2003) and Ne(Fei2007)	with annealing	XRD
Pv1008	Ruby luminescence(Dewaele2008)	cold-compressi	SMS

Table 3 Mössbauer parameters of ^{57}Fe-enriched enstatite gel

Quadrupole splittings (mm/s)	Isomer shifts (mm/s)	FWHM (mm/s)	Weight (%)
1.543(7)	0.255(3)	0.706(15)	47.5(8)
0.877(5)	0.341(3)	0.598(8)	43.17(6)
2.524(9)	0.454(4)	0.459(17)	9.4(2)

The uncertainties are given in parenthesis at the 90% confidence level for the last reported significant digit(s).

Table 4 Pressure-Volume relations of Fe^{3+}-bearing Pv and St (or $CaCl_2$-type SiO_2).

RUN #	annealing	experiments	P (GPa) using Ne scale (Fei2007)	P (GPa) using Au scale (Tsuchiya2003)	Fe^{3+}-bearing Pv a (Å)	b (Å)	c (Å)	V (Å^3)	St (or $CaCl_2$-type SiO_2) a (Å)	b (Å)	V (Å^3)
Pv0606	with annealing	XRD	30.79(8)	31.41(3)	146.27(18)	4.603(2)	4.780(2)	6.649(2)	42.82(5)	4.038(1)	4.038(1)
			36.15(4)	37.30(1)	144.61(15)	4.581(2)	4.764(2)	6.626(2)	42.29(7)	4.025(1)	4.025(1)
			40.56(1)	41.74(2)	142.81(19)	4.561(2)	4.749(2)	6.594(2)	41.84(6)	4.011(1)	4.011(1)
			43.06(6)	44.00(4)	142.07(15)	4.556(2)	4.741(2)	6.578(2)	41.55(9)	4.001(1)	4.001(1)
			46.66(10)	47.53(2)	140.66(24)	4.537(2)	4.730(2)	6.555(3)	41.26(1)	3.994(0)	3.994(0)
			50.23(2)	50.35(2)	139.60(23)	4.519(2)	4.721(2)	6.543(3)	40.99(8)	3.986(1)	3.986(1)
			52.48(13)	53.30(2)	138.92(16)	4.513(2)	4.711(2)	6.534(2)	40.76(12)	3.975(2)	3.975(2)
			55.47(11)	56.19(2)	138.05(9)	4.503(1)	4.705(1)	6.516(1)	40.57(11)	3.969(2)	3.969(2)
			57.83(11)	58.79(1)	137.37(16)	4.495(1)	4.699(2)	6.504(2)	40.37(11)	3.961(2)	3.961(2)
			61.20(10)	62.10(2)	136.38(11)	4.483(1)	4.690(1)	6.487(1)	40.14(3)	3.954(0)	3.954(0)
Pv1006	with annealing	XRD & SMS	34.06(6)	34.94(64)*	145.35(11)	4.592(1)	4.771(1)	6.634(1)	42.42(9)	4.032(1)	4.032(1)
			41.40(10)	42.25(69)*	143.10(13)	4.566(1)	4.749(1)	6.599(2)	41.75(17)	4.010(2)	4.010(2)
			64.71(10)	65.47(87)*	135.79(18)	4.474(2)	4.678(2)	6.489(3)	39.61(7)	3.998(2)	3.887(1)
			75.67(17)	76.38(98)*	132.90(27)	4.438(3)	4.648(3)	6.442(4)	38.90(37)	3.958(8)	3.865(8)
			84.85(22)	85.53(99)*	130.90(16)	4.406(2)	4.633(2)	6.412(2)	37.68(46)	3.888(9)	3.815(4)

*Normalized pressure to Au scale from Ne scale

Numbers in parentheses are standard deviation uncertainties in the last digit(s)

c (Å)
2.625(1)
2.611(1)
2.601(1)
2.596(2)
2.587(0)
2.580(1)
2.580(2)
2.576(1)
2.573(2)
2.567(1)
2.609(2)
2.596(3)
2.549(1)
2.543(3)
2.540(9)

Table 5 The equation of state parameters.

Composition	V_0	K_0	K'_0	Ref.
Mg-end member Pv	162.3	261(1)	4.0 (fixed)	Lundin *et al*. (2008)
Fe^{2+}-bearing Pv	163.3(3)	259(1)	4.0 (fixed)	Lundin *et al*. (2008)
Fe^{3+}-bearing Pv	161.5(4)	264(6)	4.0 (fixed)	This study

Numbers in parentheses are standard deviation uncertainties in the last digit.

Table 6 Mössbauer parameters of Fe^{3+}–bearing Pv

RUN #	annealing	experiments	P (GPa)		Quadrupole splittings (mm/s)	Isomer shifts (mm/s)	FWHM (mm/s)	Percent weightings (%)
Pv1006	with annealing	XRD & SMS	34.1(1)	Site 1	2.79(19)	0.95(9)	0.83(6)	18(4)
				Site 2	0.38(3)	0.25(2)	0.26(6)	78(5)
				Site 3	1.50(16)	0.48(8)	0.62(2)	4(3)
			41.4(1)	Site 1	3.23(22)	1.04(2)	1.21(13)	34(12)
				Site 2	0.48(5)	0.52(2)	1.07(68)	16(22)
				Site 3	1.55(5)	0.54(1)	2.00(41)	50(20)
			64.7(1)	Site 1	3.98(9)	0.96(5)	1.15(6)	29(7)
				Site 2	0.58(8)	0.42(2)	0.99(24)	19(13)
				Site 3	1.27(19)	0.35(8)	1.83(15)	52(12)
			75.7(2)	Site 1	4.10(10)	0.98(6)	1.13(4)	31(10)
				Site 2	0.60(9)	0.38(2)	1.18(44)	29(20)
				Site 3	1.43(20)	0.32(2)	1.77(15)	40(18)
			84.9(2)	Site 1	4.13(9)	1.03(5)	1.06(4)	27(4)
				Site 2	0.77(9)	0.39(4)	1.23(12)	42(7)
				Site 3	2.00(17)	0.35(2)	2.08(27)	31(8)
Pv1008	cold-compressi	SMS	33.3(2)	Site 1	2.79(19)	0.95(9)	0.83(6)	18(4)
				Site 2	0.38(3)	0.25(2)	0.26(6)	78(5)
				Site 3	1.50(16)	0.48(8)	0.62(2)	4(3)
			37.6(6)	Site 1	2.90(24)	0.95(2)	0.84(7)	16(5)
				Site 2	0.40(4)	0.24(2)	0.19(5)	81(5)
				Site 3	1.51(13)	0.45(6)	0.67(2)	3(3)

39.9(7)	Site 1	2.94(35)	1.10(9)	1.11(16)	13(7)
	Site 2	0.41(5)	0.21(2)	0.19(12)	86(8)
	Site 3	1.51(31)	0.33(5)	0.72(3)	1(4)
46.8(2)	Site 1	3.08(31)	0.93(7)	0.71(9)	11(5)
	Site 2	0.41(4)	0.18(2)	0.59(3)	85(10)
	Site 3	1.56(67)	0.35(4)	0.66(2)	4(10)
63.8(8)	Site 1	3.20(42)	1.05(9)	1.30(13)	20(7)
	Site 2	0.37(6)	0.14(2)	0.19(7)	78(7)
	Site 3	1.64(19)	0.33(9)	0.69(3)	2(3)

The uncertainties are given in parenthesis at the 90% confidence level for the last reported significant digit(s).